Supplementary for: Reduced effective radiative forcing from cloud-aerosol interactions (ERF_{aci}) with improved treatment of early aerosol growth in an Earth System Model

Sara Marie Blichner[1], **Moa Kristina Sporre**[2], **and Terje Koren Berntsen**[1]

[1]Departmenet of Geosciences and Centre for Biogeochemistry in the Anthroposcene, University of Oslo, Oslo, Norway
[2]Department of Physics, Lund University, Lund, Sweden

Correspondence: Sara Marie Blichner (s.m.blichner@geo.uio.no)

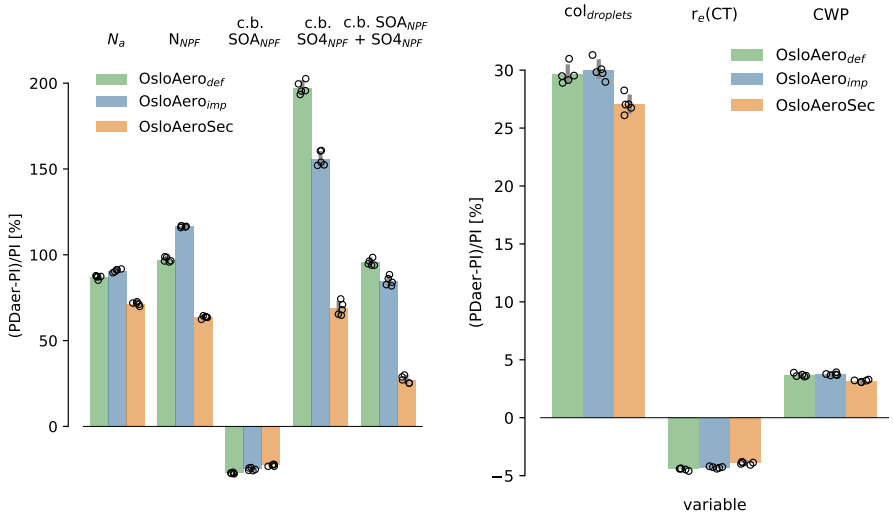

Figure S1. Globally averaged change in aerosol and cloud properties. N_{NPF} and N_a values are averaged up to 850 hPa and weighted by pressure difference of the grid cell.

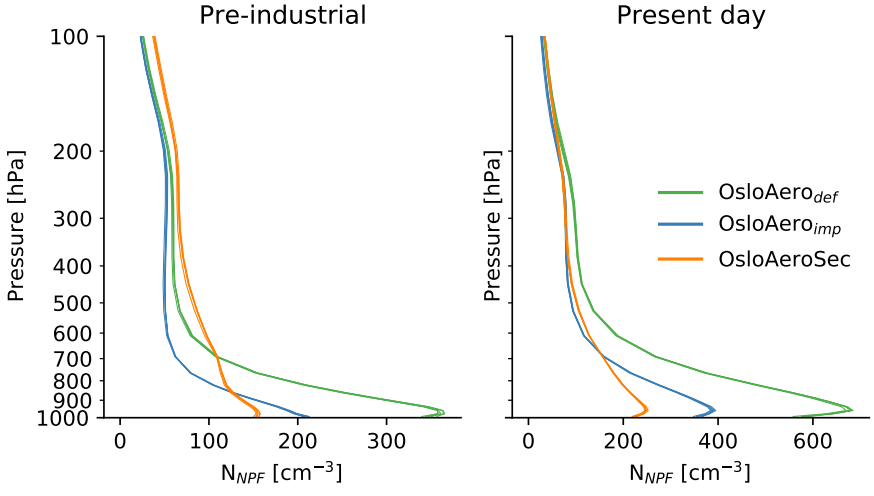

Figure S2. Globally averaged concentration of aerosols from NPF for pre-industrial (left) and present day (right) aerosols. The individual lines represent the annual average of each year in each simulation.

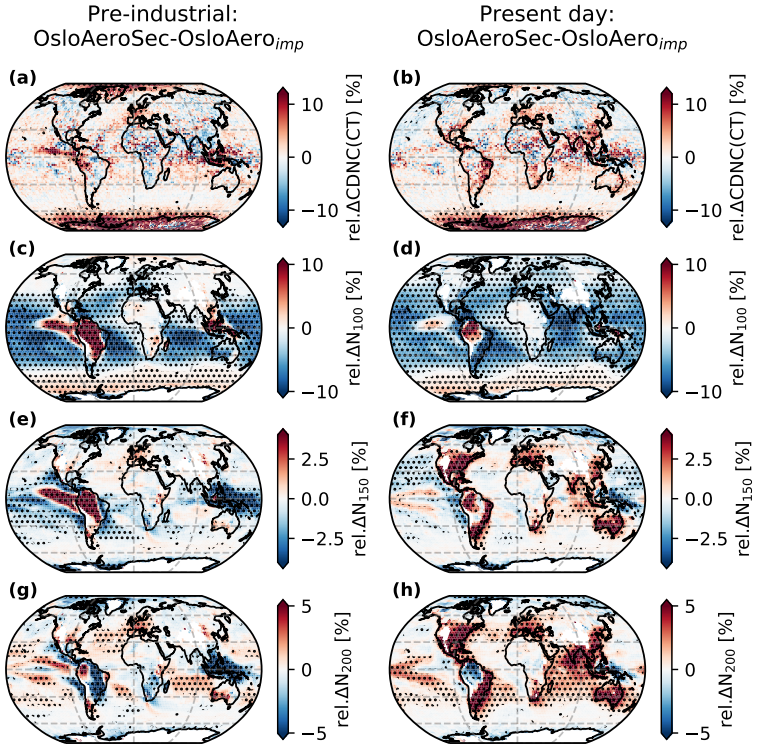

Figure S3. Top row: Difference in average cloud droplet number concentrations (CDNC) at cloud top between OsloAeroSec and OsloAero$_{def}$. Row 2–3: difference in average particle number concentration for particles larger than 100 nm (row 2), 150 nm (row 3) and 200 nm (row 4). The left column shows the difference for the pre-industrial atmosphere and the right column shows the difference for the present day atmosphere. The average particle concentrations are calculated averaging up to 850 hPa and averaging by pressure difference. Dots are included in the plots to indicate where the difference between the two models is significant with a two-tailed paired Student's t–test with 95 % confidence interval.

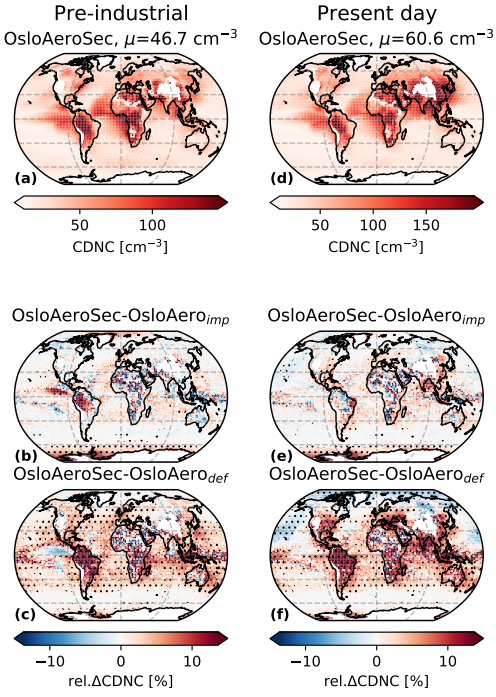

Figure S4. Top row: Near surface CDNC in OsloAeroSec for PI and PD atmosphere. Row 2 and 3 show the difference between OsloAeroSec and OsloAero$_{imp}$ and OsloAero$_{def}$ respectively. The average is calculated for grid boxes up to 850 hPa and averaging by pressure difference. Dots are included in the plots to indicate where the difference between the two models is significant with a two-tailed paired Student's t–test with 95 % confidence interval.

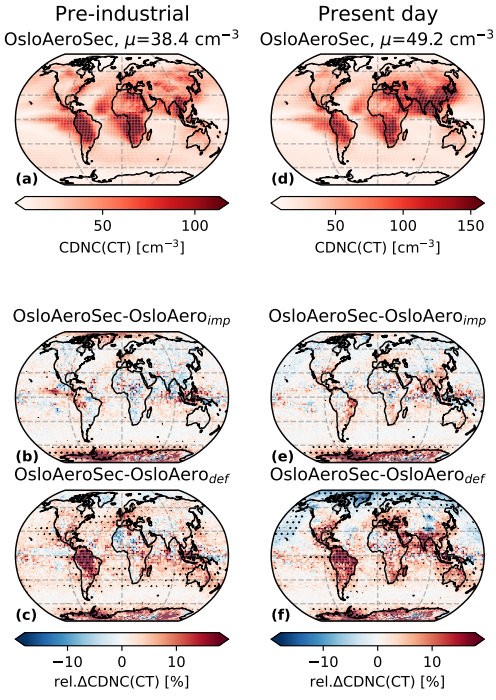

Figure S5. Top row: Cloud top CDNC in OsloAeroSec for PI and PD atmosphere. Row 2 and 3 show the difference between OsloAeroSec and OsloAero$_{imp}$ and OsloAero$_{def}$ respectively.

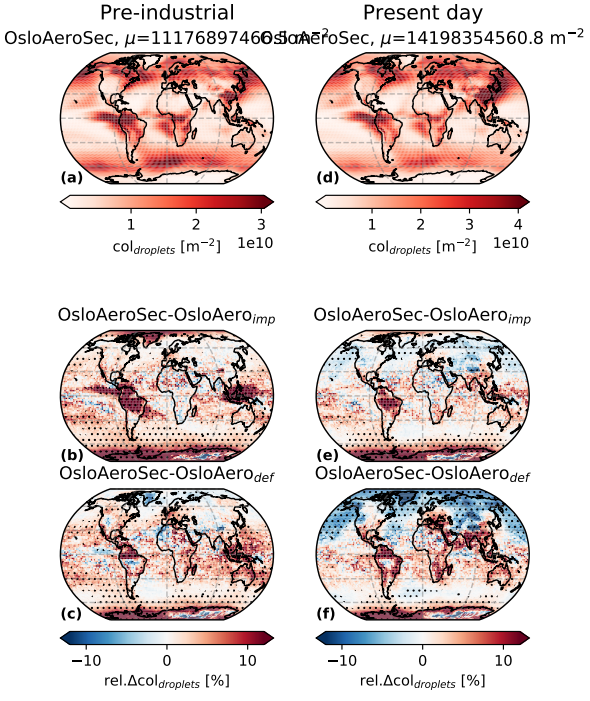

Figure S6. Top row: Column integrated droplet number in OsloAeroSec for PI and PD atmosphere. Row 2 and 3 show the difference between OsloAeroSec and OsloAero$_{imp}$ and OsloAero$_{def}$ respectively. Dots are included in the plots to indicate where the difference between the two models is significant with a two-tailed paired Student's t–test with 95 % confidence interval.

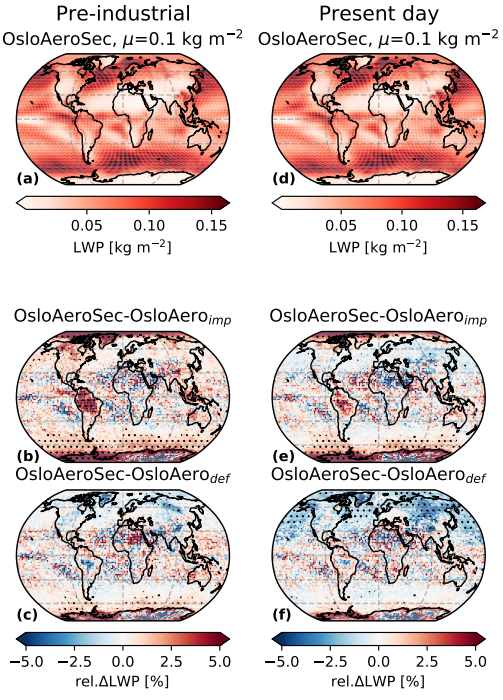

Figure S7. Top row: Liquid water path (LWP) OsloAeroSec for PI and PD atmosphere. Row 2 and 3 show the difference between OsloAeroSec and OsloAero$_{imp}$ and OsloAero$_{def}$ respectively. Dots are included in the plots to indicate where the difference between the two models is significant with a two-tailed paired Student's t–test with 95 % confidence interval.

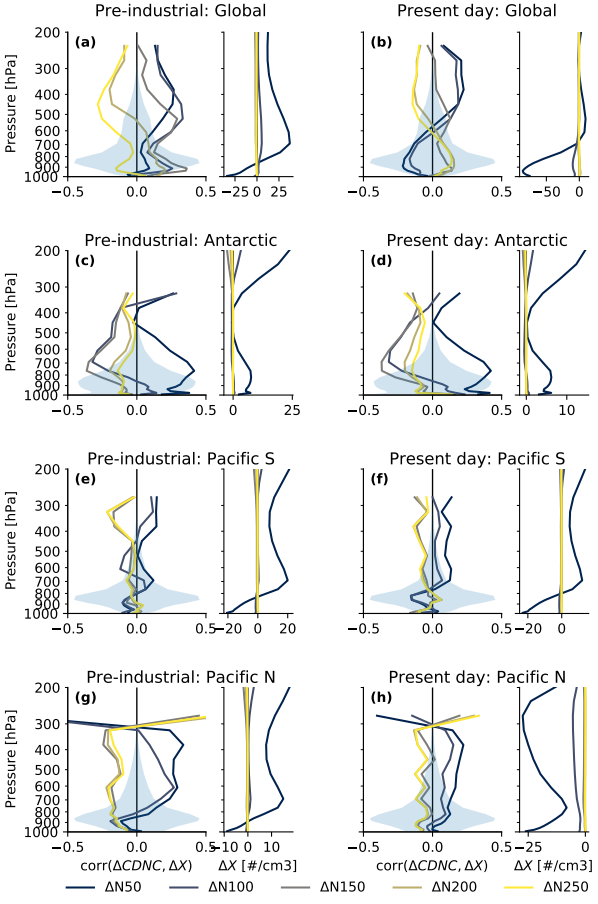

Figure S8. Left panel of each subplot: Correlations by pressure level between the change between OsloAero$_{def}$ and OsloAeroSec in cloud droplet number concentration (ΔCDNC) and the change in number of particles above 50, 100, 150,200 and 250 nm for different regions. The blue shaded signifies the relative fractional occurrence of liquid cloud and is included to give an idea of where the aerosols may actually have a noticeable impact on clouds. The right panel of each subplot shows the change in the aerosol concentration for the relevant region.

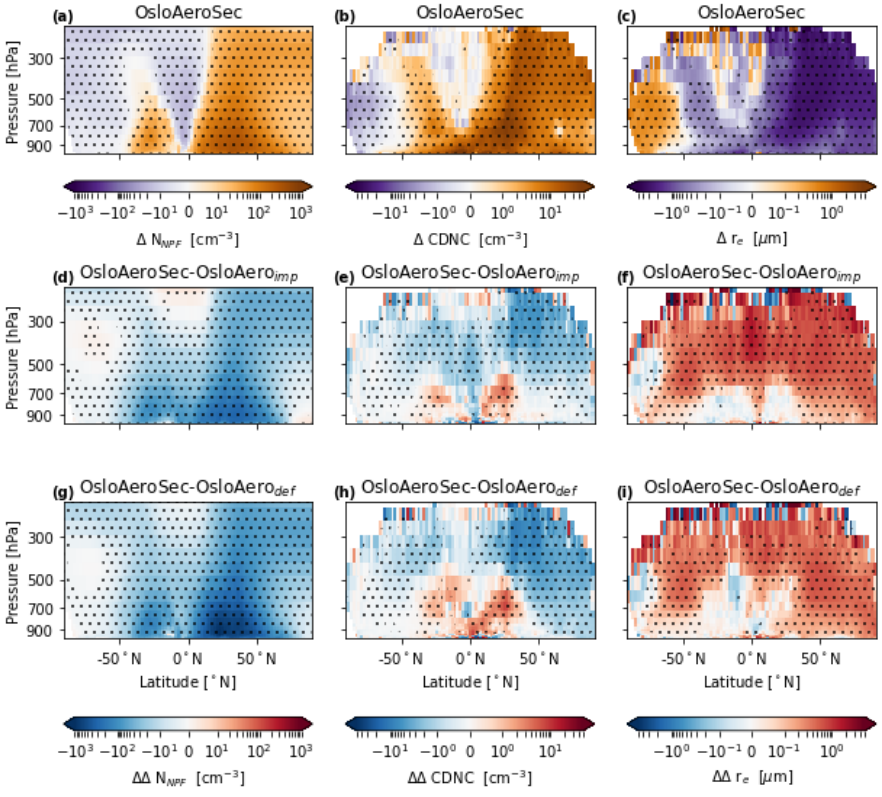

Figure S9. Zonally averaged values for N_{NPF}, cloud droplet number concentration (CDNC) and effective droplet radius (r_e). The top panel shows the PD - PI for OsloAeroSec while the second and third row shows the of this value to the value with OsloAero$_{imp}$ (second row) and OsloAero$_{def}$ (third row). Dots are included in the plots to indicate where the difference between the two models is significant with a two-tailed paired Student's t–test with 95 % confidence interval.

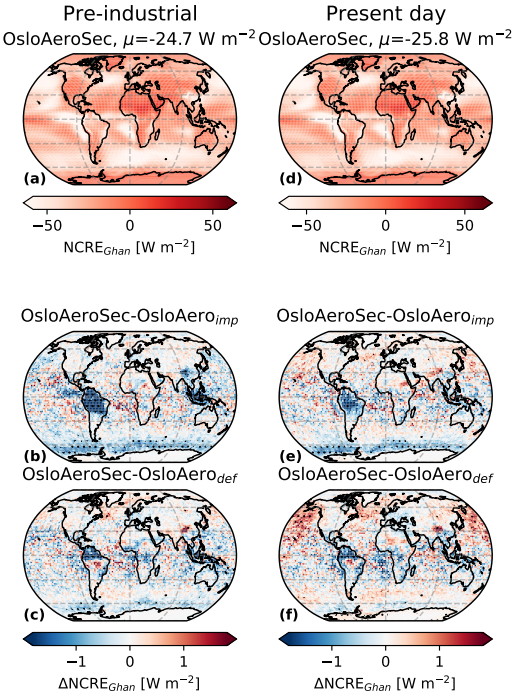

Figure S10. Top row: NCRE$_{Ghan}$ in OsloAeroSec for PI and PD atmosphere. Row 2 and 3 show the difference between OsloAeroSec and OsloAero$_{imp}$ and OsloAero$_{def}$ respectively. Dots are included in the plots to indicate where the difference between the two models is significant with a two-tailed paired Student's t–test with 95 % confidence interval.

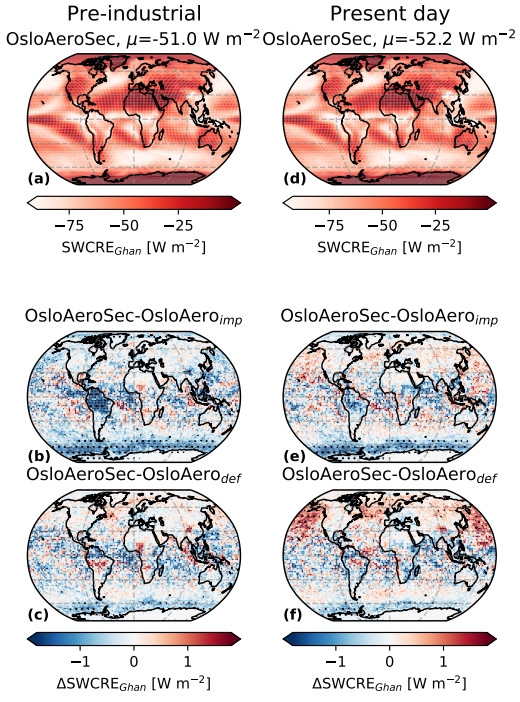

Figure S11. Top row: Short wave CRE in OsloAeroSec for PI and PD atmosphere. Row 2 and 3 show the difference between OsloAeroSec and OsloAero$_{imp}$ and OsloAero$_{def}$ respectively. Dots are included in the plots to indicate where the difference between the two models is significant with a two-tailed paired Student's t–test with 95 % confidence interval.

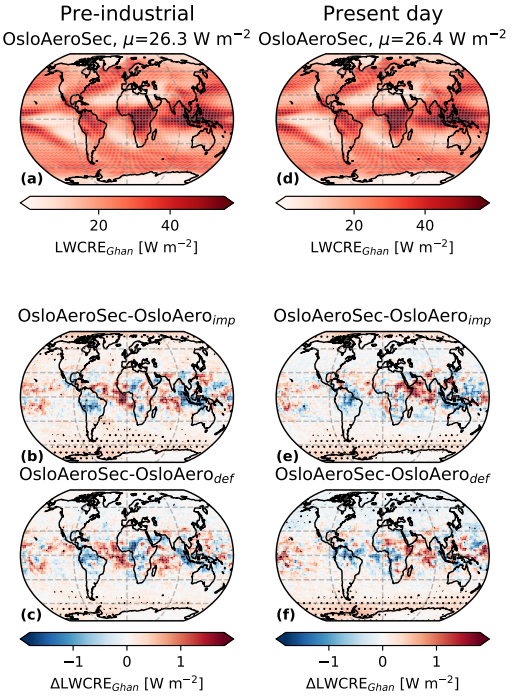

Figure S12. Top row: Long wave CRE in OsloAeroSec for PI and PD atmosphere. Row 2 and 3 show the difference between OsloAeroSec and OsloAero$_{imp}$ and OsloAero$_{def}$ respectively. Dots are included in the plots to indicate where the difference between the two models is significant with a two-tailed paired Student's t–test with 95 % confidence interval.

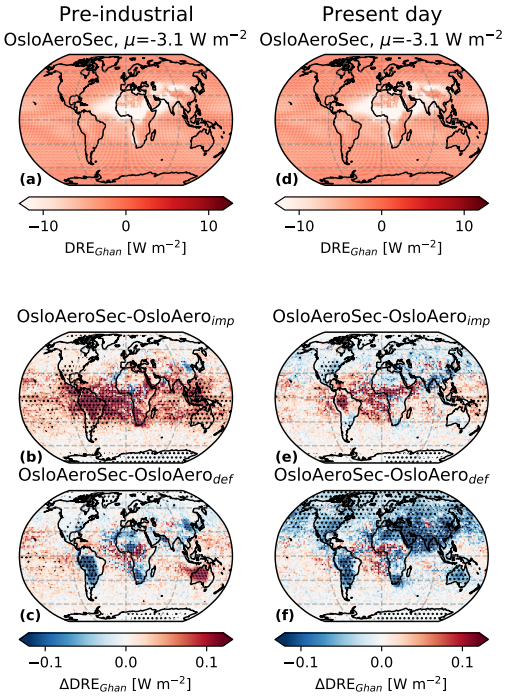

Figure S13. Top row: The direct radiative effect in OsloAeroSec for PI and PD atmosphere. Row 2 and 3 show the difference between OsloAeroSec and OsloAero$_{imp}$ and OsloAero$_{def}$ respectively. Dots are included in the plots to indicate where the difference between the two models is significant with a two-tailed paired Student's t–test with 95 % confidence interval.

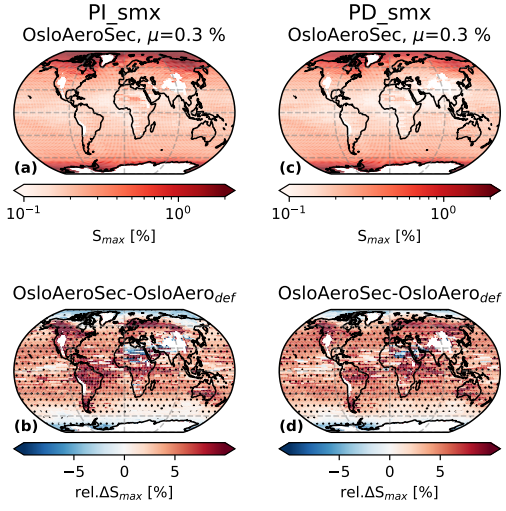

Figure S14. Top row:Average values of maximum supersaturation (S$_{max}$) for OsloAeroSec for PI (left) and PD (right). Row 2–3: the relative difference between OsloAeroSec and OsloAero$_{imp}$ (row 2) and OsloAero$_{def}$ (row 3) for PI (left) and PD(right). All values are averaged up to 850 hPa and weighted by pressure difference of the grid cell. Furthermore, only values where S$_{max}$ is larger than zero are counted towards the average. Dots are included in the plots to indicate where the difference between the two models is significant with a two-tailed paired Student's t–test with 95 % confidence interval.

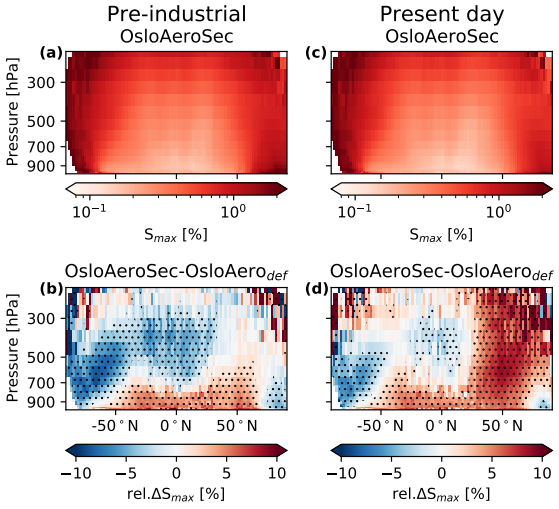

Figure S15. Top row:Average values of maximum supersaturation (S_{max} for OsloAeroSec for PI (left) and PD (right). Bottom row: the relative difference between OsloAeroSec and OsloAero$_{def}$ for PI (left) and PD(right). Only values where S_{max} is larger than zero are counted towards the average. Dots are included in the plots to indicate where the difference between the two models is significant with a two-tailed paired Student's t–test with 95 % confidence interval.

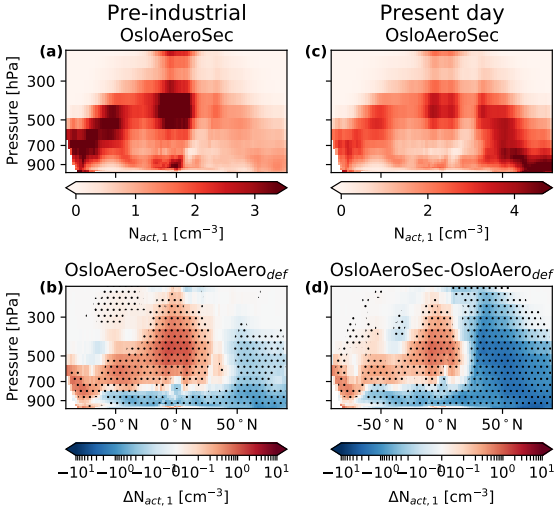

Figure S16. Top row: Average values of the averaged activation of particles from the NPF mode (mix number 1) for OsloAeroSec for PI (left) and PD (right). Bottom row: the relative difference between OsloAeroSec and OsloAero$_{def}$ for PI (left) and PD(right). The values are an approximation in the sense that they are calculated by multiplying the separately calculated monthly mean output of the number concentration in the mode and the activation fraction from that mode (see Fig. S18). Dots are included in the plots to indicate where the difference between the two models is significant with a two-tailed paired Student's t–test with 95 % confidence interval.

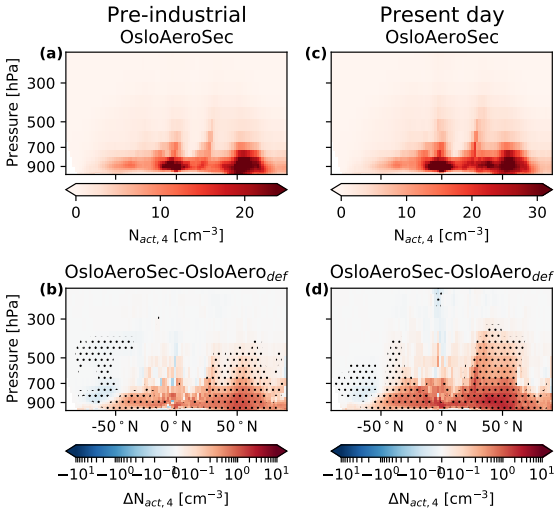

Figure S17. Top row: Average values of the averaged activation of particles from mode number 4 (mix number 4) for OsloAeroSec for PI (left) and PD (right). Bottom row: the relative difference between OsloAeroSec and OsloAero$_{def}$ for PI (left) and PD(right). The values are an approximation in the sense that they are calculated by multiplying the separately calculated monthly mean output of the number concentration in the mode and the activation fraction from that mode (see Fig. S19). Dots are included in the plots to indicate where the difference between the two models is significant with a two-tailed paired Student's t–test with 95 % confidence interval.

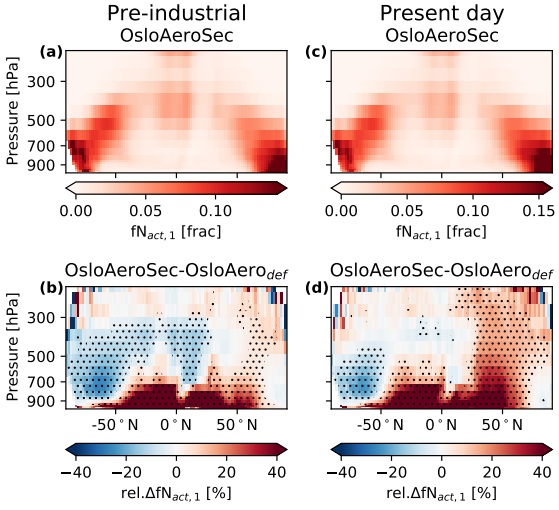

Figure S18. Top row: Average values of the activated fraction of particles from the NPF mode (mix number 1) for OsloAeroSec for PI (left) and PD (right). Bottom row: the relative difference between OsloAeroSec and OsloAero$_{def}$ for PI (left) and PD(right). The values are an approximation in the sense that they are calculated by multiplying the separately calculated monthly mean output of the number concentration in the mode and the activation fraction from that mode. Dots are included in the plots to indicate where the difference between the two models is significant with a two-tailed paired Student's t–test with 95 % confidence interval.

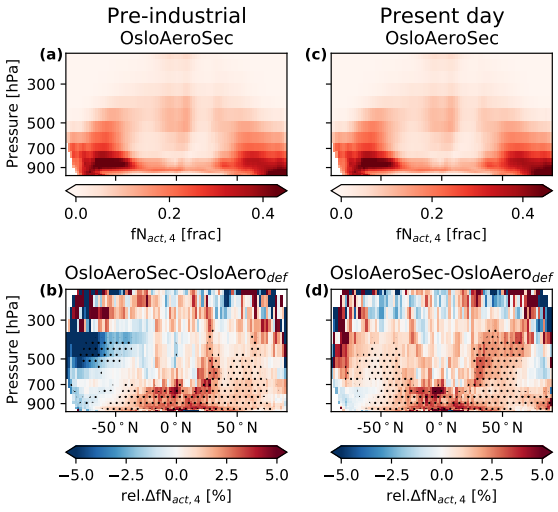

Figure S19. Top row: Average values of the activated fraction of particles from mode number 4 (mix number 4) for OsloAeroSec for PI (left) and PD (right). Bottom row: the relative difference between OsloAeroSec and OsloAero$_{def}$ for PI (left) and PD(right). Dots are included in the plots to indicate where the difference between the two models is significant with a two-tailed paired Student's t–test with 95 % confidence interval.

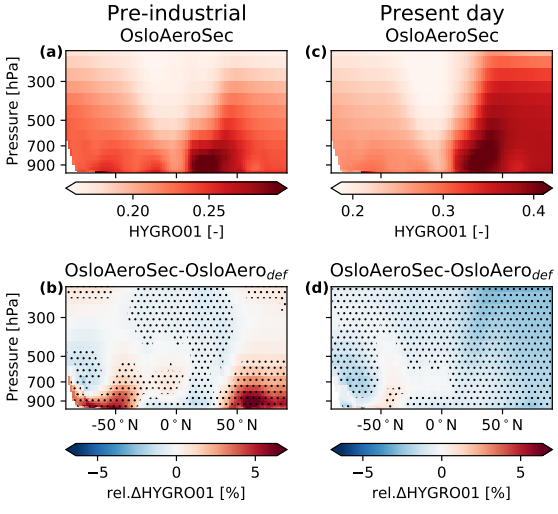

Figure S20. Top row: Average values of the hygroscopicity particles from mode number 1 (mix number 1) for OsloAeroSec for PI (left) and PD (right). Bottom row: the relative difference between OsloAeroSec and OsloAero$_{def}$ for PI (left) and PD(right). Dots are included in the plots to indicate where the difference between the two models is significant with a two-tailed paired Student's t–test with 95 % confidence interval.

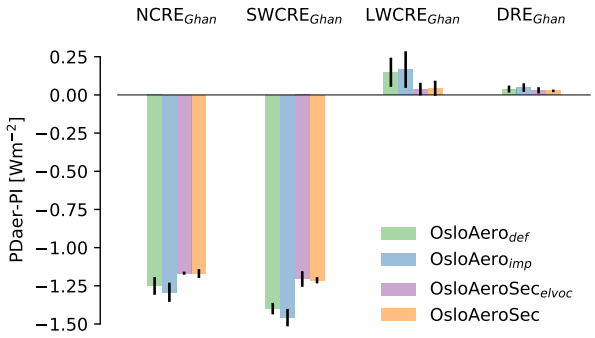

Figure S21. Globally averaged ERF for 1 year (plus one spin-up year) of simulations. The OsloAeroSec$_{elvoc}$ case is a sensitivity simulation were only 50% of ELVOC is allowed to condense onto the particles in the sectional scheme. The simulation was run to test the influence of this factor on the overall results in the paper.

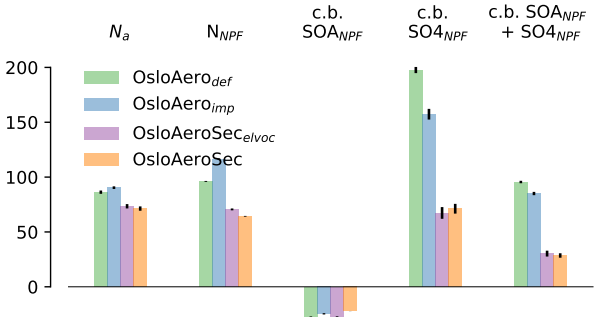

Figure S22. Globally averaged aerosol properties for 1 year (plus one spin-up year) of simulations. The OsloAeroSec$_{elvoc}$ case is a sensitivity simulation were only 50% of ELVOC is allowed to condense onto the particles in the sectional scheme. The simulation was run to test the influence of this factor on the overall results in the paper.

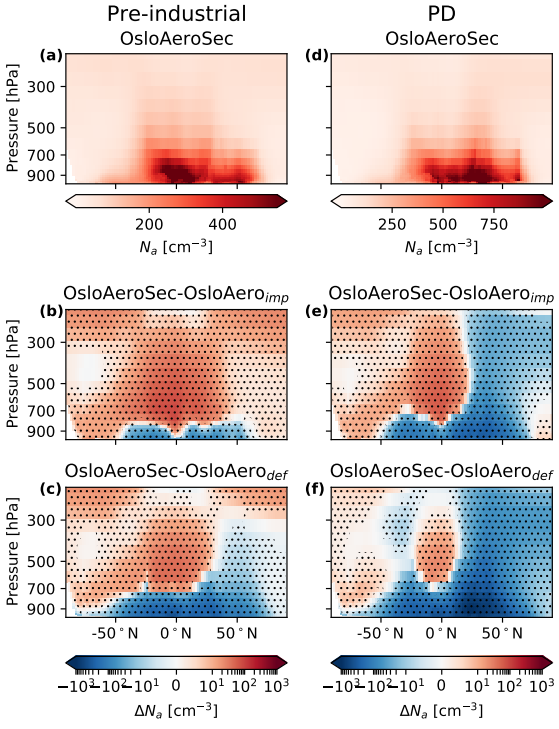

Figure S23. Zonally averaged values for N$_a$. The top panel shows the absolute values in the Pre-industrial (left) and Present day (right) atmosphere) PD - PI for OsloAeroSec while the second and third row shows the of this value to the value with OsloAero$_{imp}$ (second row) and OsloAero$_{def}$ (third row). Dots are included in the plots to indicate where the difference between the two models is significant with a two-tailed paired Student's t–test with 95 % confidence interval.

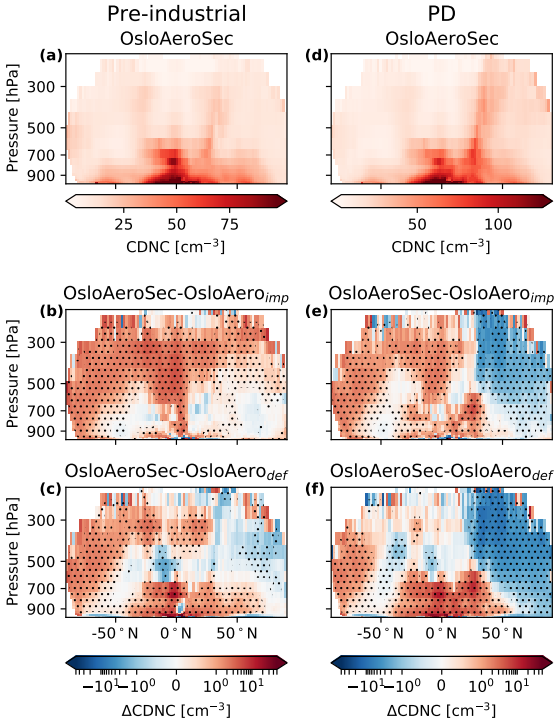

Figure S24. Zonally averaged values for cloud droplet number concentrations. The top panel shows the absolute values in the Pre-industrial (left) and Present day (right) atmosphere) PD - PI for OsloAeroSec while the second and third row shows the of this value to the value with OsloAero$_{imp}$ (second row) and OsloAero$_{def}$ (third row). Dots are included in the plots to indicate where the difference between the two models is significant with a two-tailed paired Student's t–test with 95 % confidence interval.